Supplementary information

Dynamics of groundwater-land surface response times as a dryland flash drought diagnosis

Hoang Hai Nguyen[1], Di Long[2], S.-Y. Simon Wang[2], Jinho Yoon[1], Yulong Zhong[3], Hyunglok Kim[1*]

[1]Department of Environment and Energy Engineering, Gwangju Institute of Science and Technology, Gwangju, Republic of Korea

[2]Department of Hydraulic Engineering, Tsinghua University, Beijing, China

[3]Department of Agronomy, Kasetsart University, Bangkok, Thailand

[4]School of Geography and Information Engineering, China University of Geosciences (Wuhan), Wuhan, China

*Corresponding author: hyunglokkim@gist.ac.kr

This SI file includes:

Supplementary Figures 1 to **16**

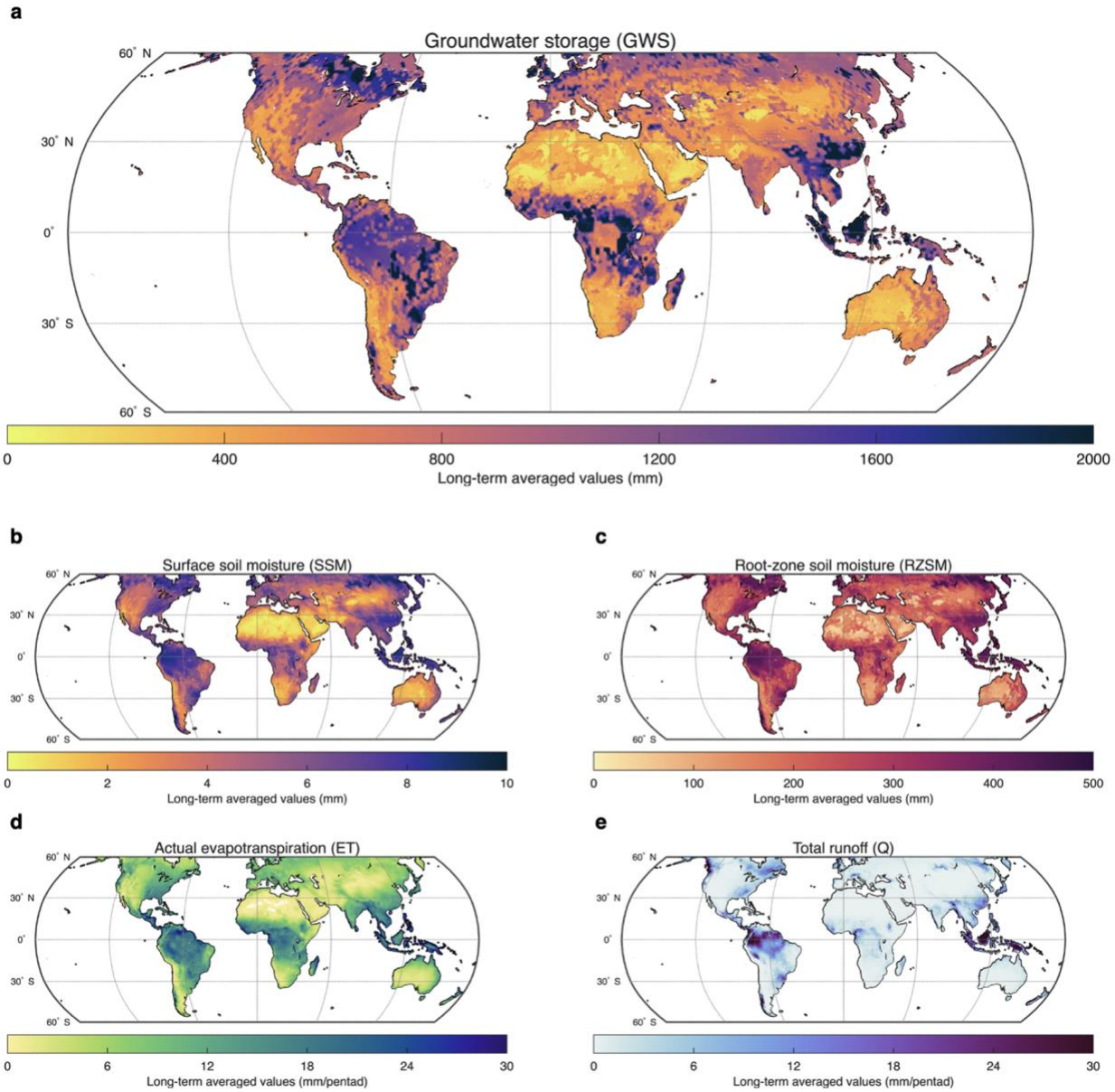

Supplementary Fig. 1.
Spatial distributions of the long-term (20 years, 2004-2023) averages for major hydroclimate variable datasets from the GLDAS-2.2 GRACE-DA product. a, Groundwater storage (GWS, variable *GWS_tavg* in the product). **b,** Surface soil moisture (SSM, variable *SoilMoist_S_tavg* in the product). **c,** Root-zone soil moisture (RZSM, variable *SoilMoist_RZ_tavg* in the product). **d,** Actual evapotranspiration (ET, variable *Evap_tavg* in the product). **e,** Total runoff (Q), derived as the sum of surface runoff (Q_s, variable *Qs_tavg* in the product) and baseflow runoff (Q_{sb}, variable *Qsb_tavg* in the product).

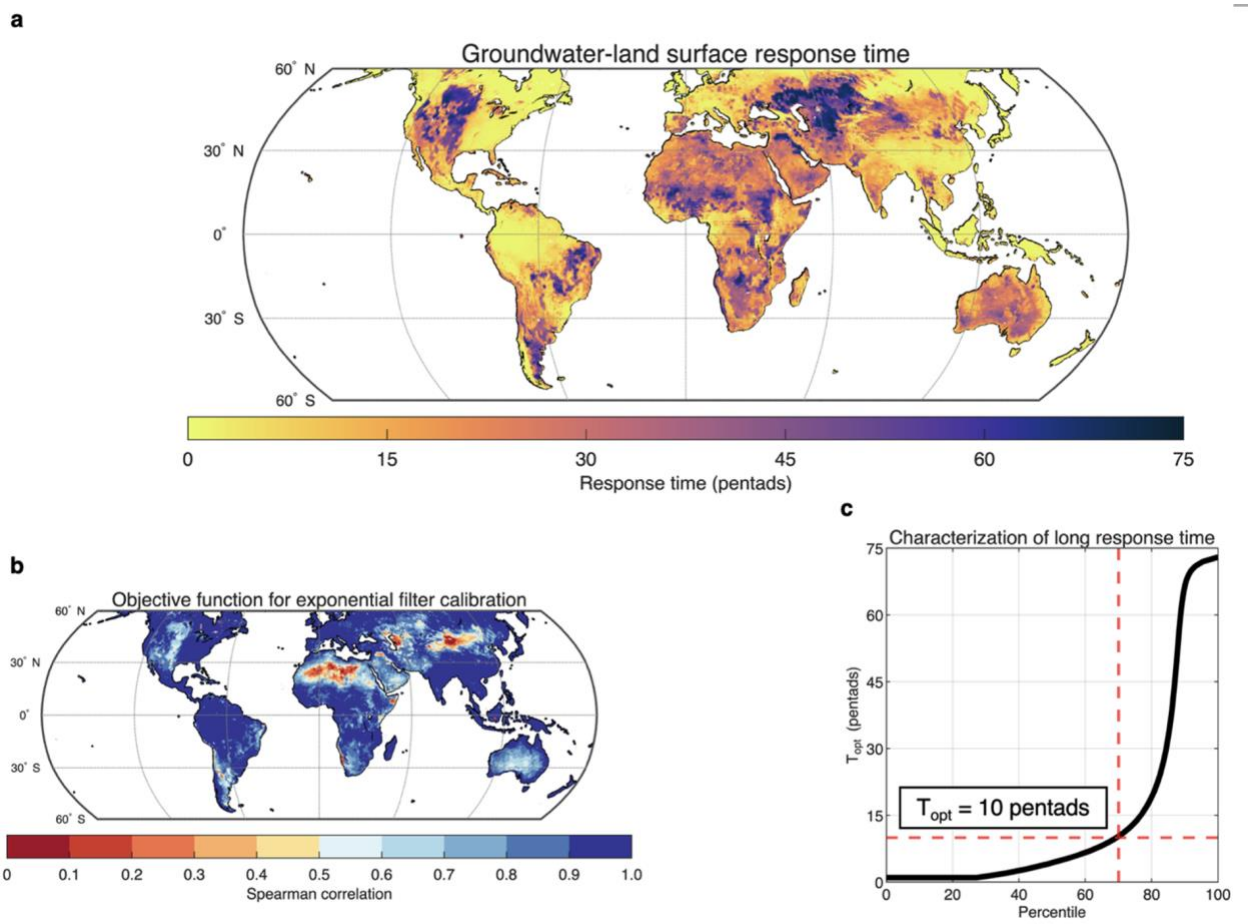

Supplementary Fig. 2.
Groundwater-land surface response time (groundwater response time, T_{opt}) generated from the dynamic exponential filter model. a, Spatial distribution of the long-term averages of T_{opt}, characterized by calibrating the dynamic exponential filter model to the SSM and GWS data, where SSM and GWS are regarded as the first and second soil layers, respectively. **b,** Spatial distribution of the long-term averages of Spearman's correlation coefficient (R) used as the objective function for calibrating the dynamic exponential filter model and masking T_{opt} data. **c,** Characterization of long groundwater response time, given that the criterion for this characterization is based on the global T_{opt} distribution, with T_{opt} values exceeding the 70^{th} percentile.

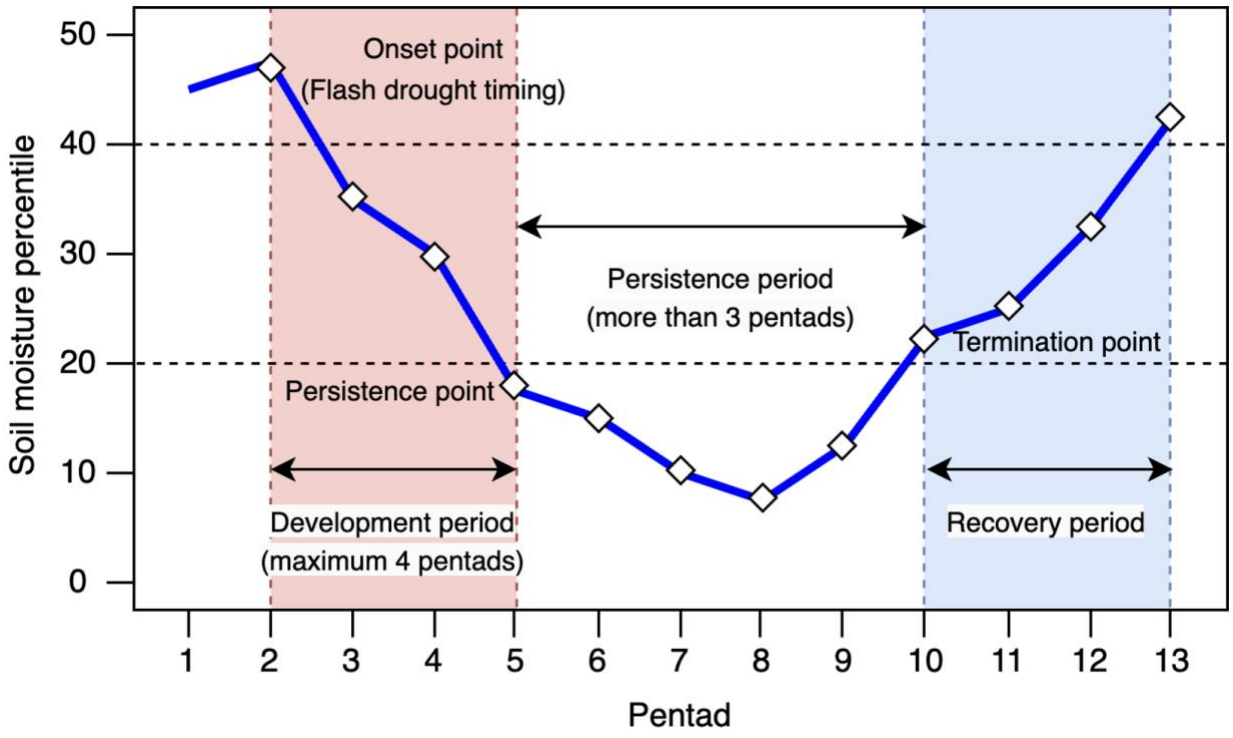

Supplementary Fig. 3.
Methodology for flash drought characterization. An illustration of a flash drought event identification methodology with its main characteristics.

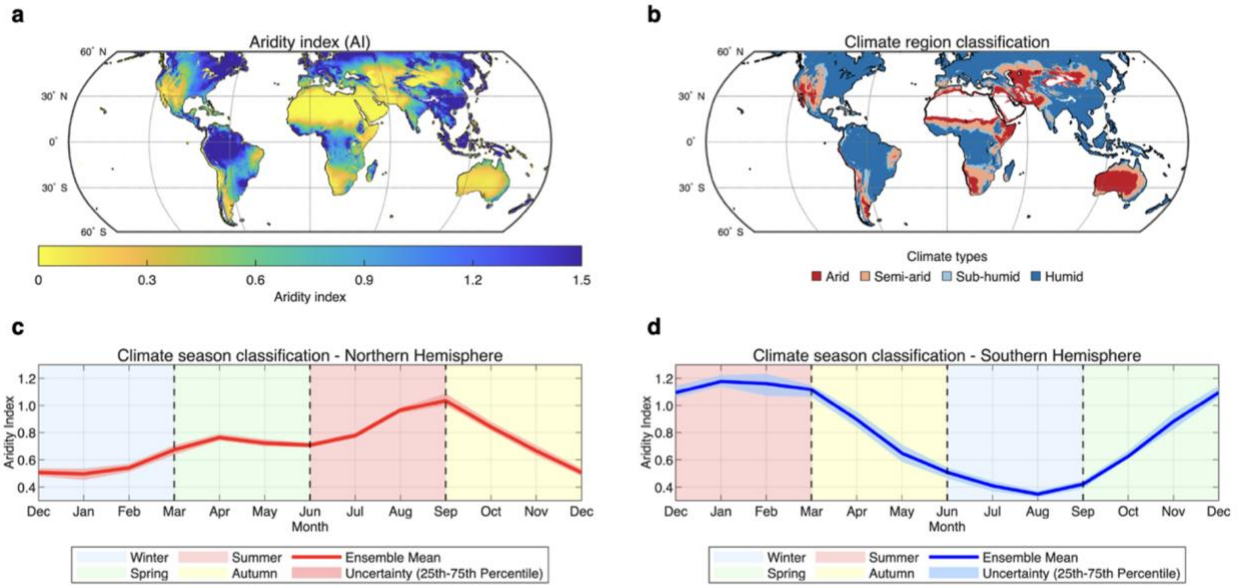

Supplementary Fig. 4.

Spatiotemporal aridity index (AI) with climate region and season classifications. a, Spatial distribution of long-term annual AI averages; **b,** Spatial distribution of climate region classifications based on the long-term annual AI averages, including arid ($0.05 < AI \leq 0.20$), semi-arid ($0.20 < AI \leq 0.50$), dry sub-humid ($0.50 < AI \leq 0.65$), and humid climate regions ($0.65 \leq AI$). **c, d,** Monthly variation of AI averages with climate season classifications for **c,** Northern Hemisphere, and **d,** Southern Hemisphere, including the winter (blue block), spring (green block), summer (red block), and autumn (yellow block), with the red and blue bold lines representing the ensemble mean of all pixels in the Northern and Southern Hemispheres, respectively, and shaded areas representing the uncertainty ranges between 25th and 75th percentiles.

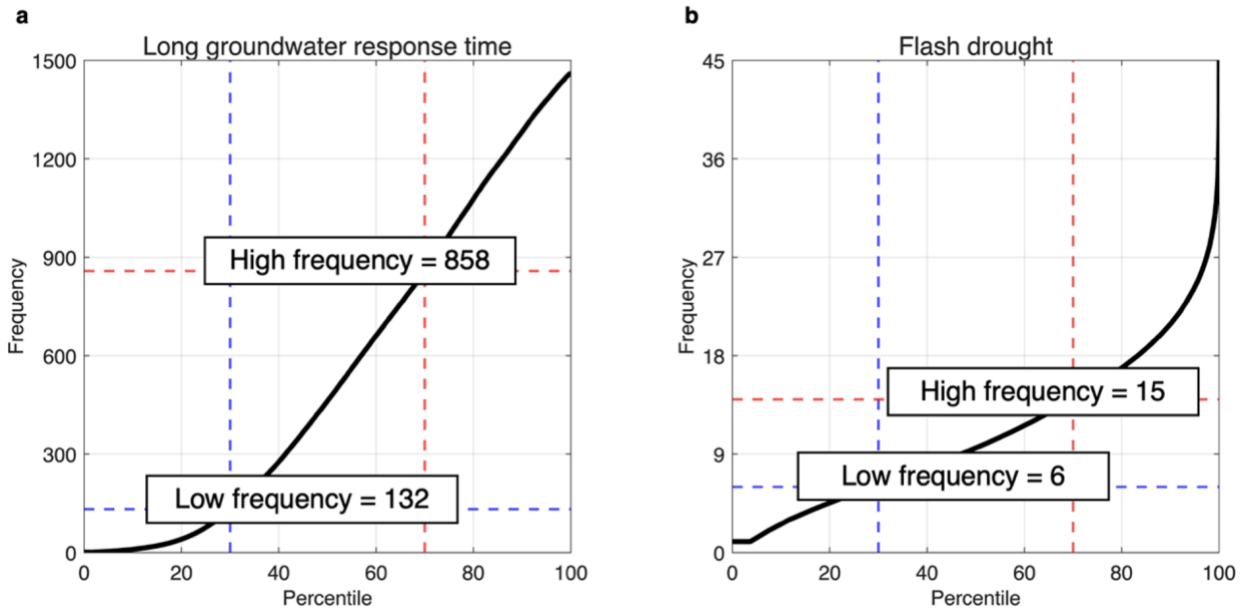

Supplementary Fig. 5.
Characterization of high and low frequencies for long groundwater response time (T_{opt}) and flash drought. a, b, Characterization of **a,** long groundwater response time frequency, and **b,** flash drought frequency over different percentiles for selecting high and low frequencies. The red and blue dashed lines represent the thresholds for these high and low frequencies, given the frequency values of the 70th and 30th percentiles, respectively.

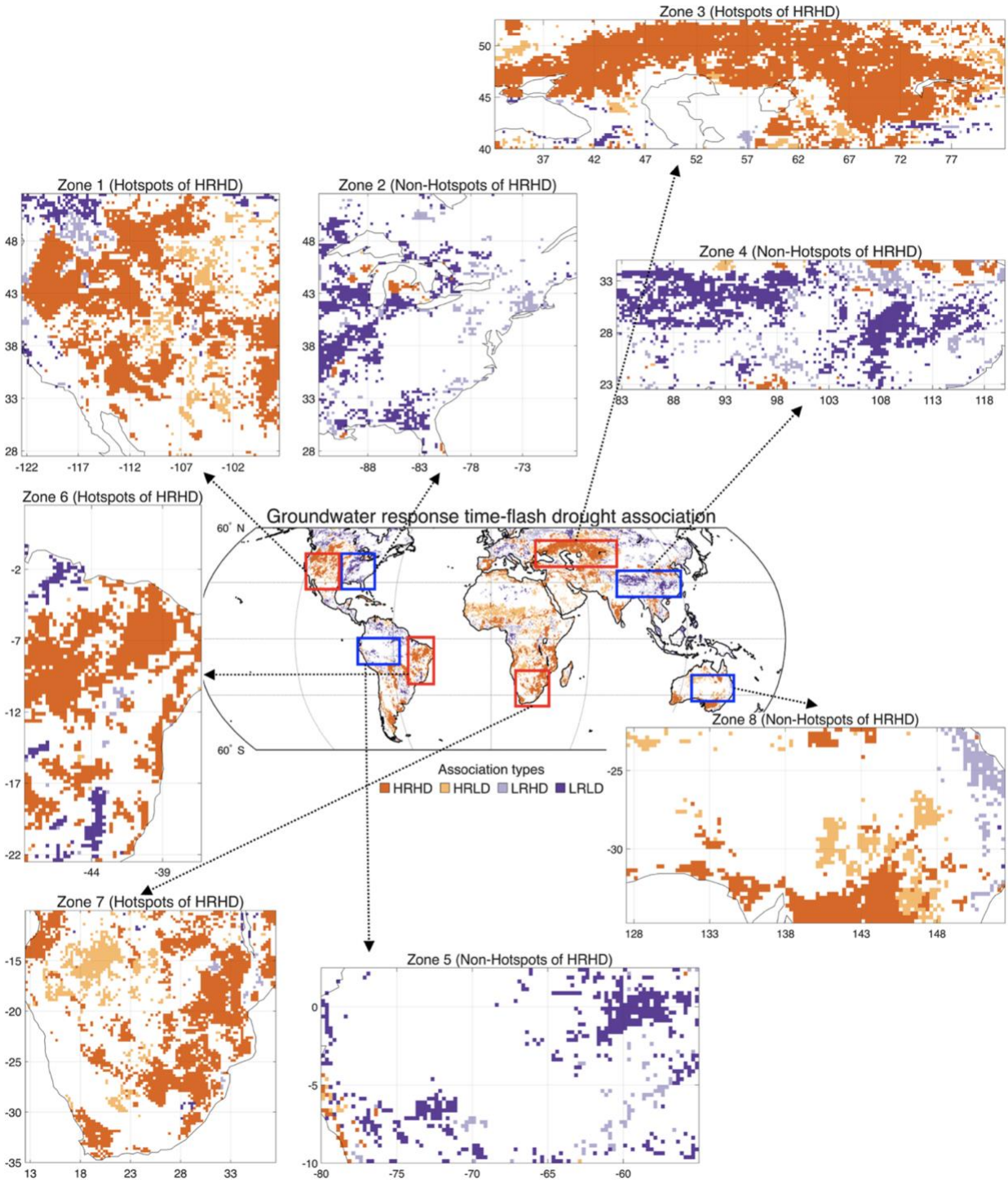

Supplementary Fig. 6.
Selected hotspots and non-hotspots of high association of long groundwater response time and frequent flash drought (HRHD). A total of eight zones are selected, including four zones in the Northern Hemisphere (Zone 1, 2, 3, and 4) and four zones in the Southern Hemisphere (Zone 5, 6, 7, and 8), with four hotspot areas of HRHD (red rectangle; Zone 1, 3, 6, and 7) and four non-hotspot areas of HRHD (blue rectangle; Zone 2, 4, 5, and 8).

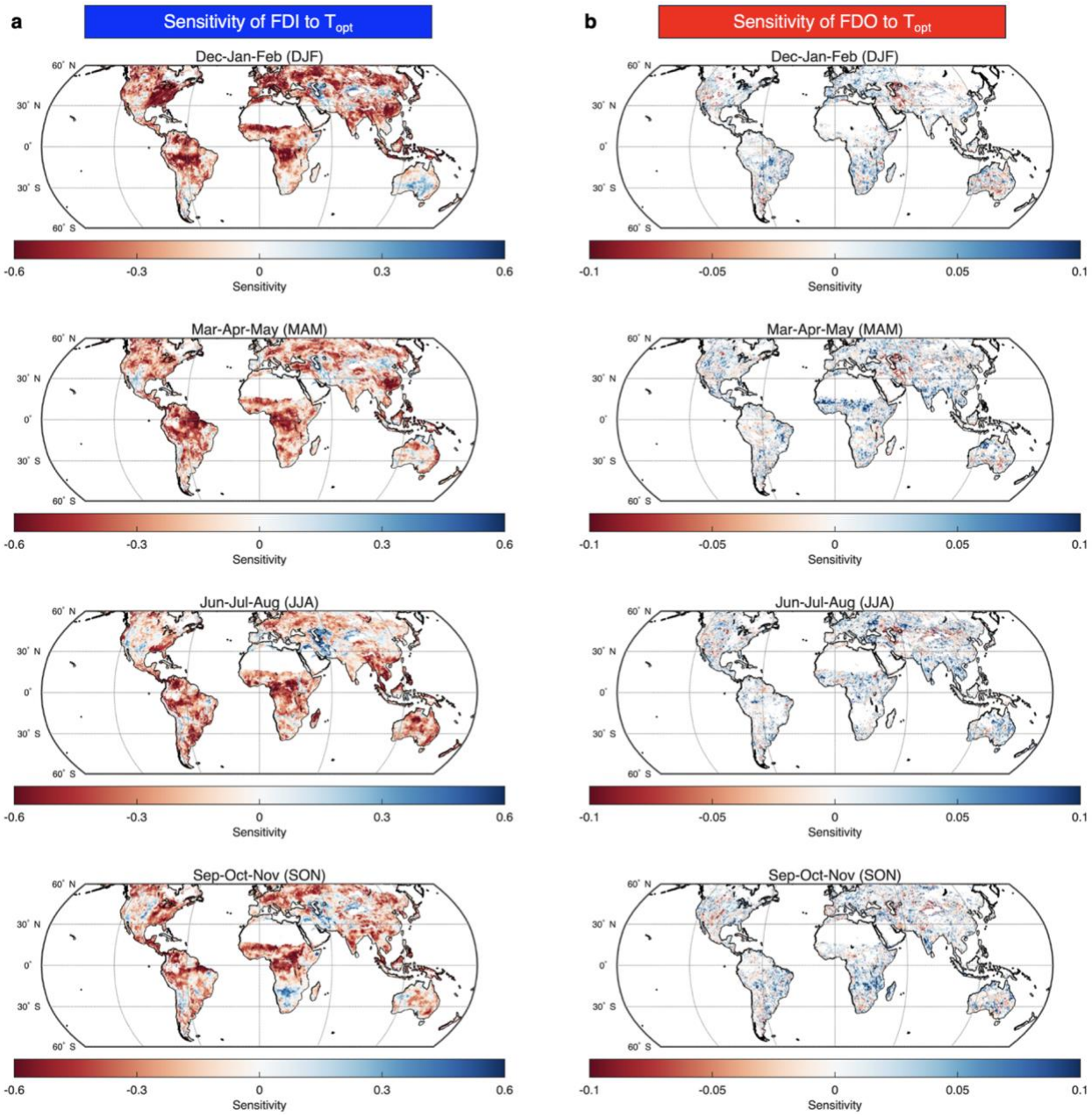

Supplementary Fig. 7.
Spatial distributions of seasonal sensitivities of the flash drought characteristics to groundwater response time (T_{opt}) (inverse of Fig. 3). a, Sensitivities of the RZSM percentile-based flash drought indicator (FDI) to T_{opt} over Dec-Jan-Feb (DJF), Mar-Apr-May (MAM), Jun-Jul-Aug (JJA), and Sep-Oct-Nov (SON) (left panel). **b,** Sensitivities of flash drought onset (FDO) to T_{opt} over DJF, MAM, JJA, and SON (right panel).

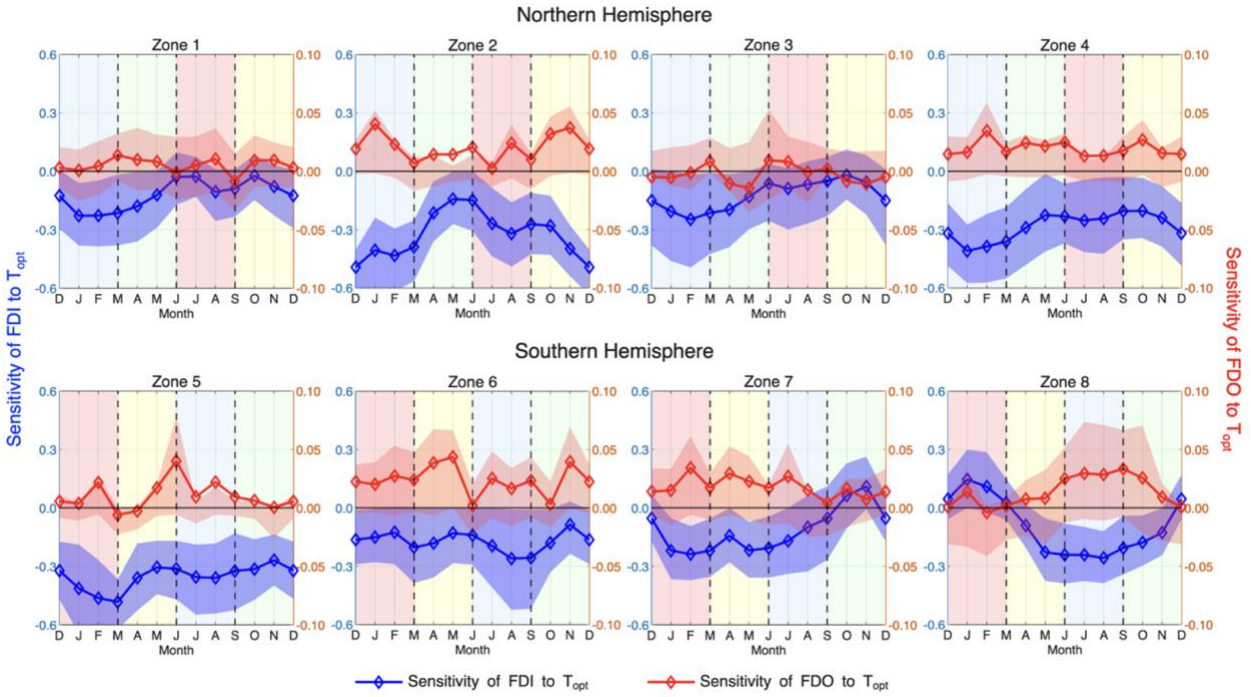

Supplementary Fig. 8.
Monthly variation of seasonal sensitivities of flash drought characteristics to groundwater response time (T_{opt}) for selected zones (inverse of Fig. 4). Monthly sensitivities of the RZSM percentile-based flash drought indicator (FDI) to T_{opt} (blue marker lines and shaded areas) and monthly sensitivities of flash drought onset (FDO) to T_{opt} (red marker lines and shaded areas) for four selected zones in the Northern Hemisphere, including hotspots (Zone 1 and 3) and non-hotspots (Zone 2 and 4) (upper panel), and four selected zones in the Southern Hemisphere, including hotspots (Zone 6 and 7) and non-hotspots (Zone 5 and 8) (lower panel), as characterized in Supplementary Fig. 6. The marker lines represent the ensemble mean of all pixels within the selected zones, and the shaded areas represent the uncertainty ranges between the 25th and 75th percentiles.

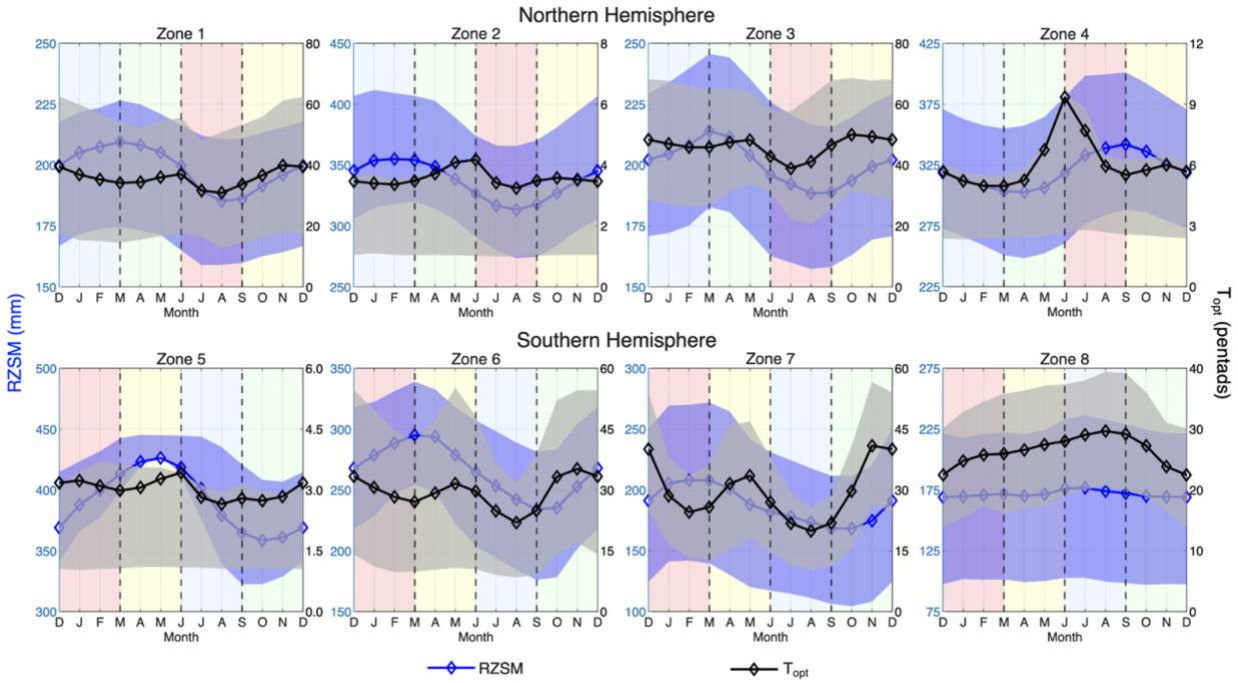

Supplementary Fig. 9.
Monthly variation of soil wetness conditions and groundwater response time (T_{opt}) for selected zones. Monthly RZSM values (in mm, blue marker lines and shaded areas) and corresponding monthly T_{opt} values (in pentads, black marker lines and shaded areas) for four selected zones in the Northern Hemisphere, including hotspots (Zone 1 and 3) and non-hotspots (Zone 2 and 4) (upper panel), and four selected zones in the Southern Hemisphere, including hotspots (Zone 6 and 7) and non-hotspots (Zone 5 and 8) (lower panel), as characterized in Supplementary Fig. 6. The marker lines represent the ensemble mean of all pixels within the selected zones, and the shaded areas represent the uncertainty ranges between the 25th and 75th percentiles.

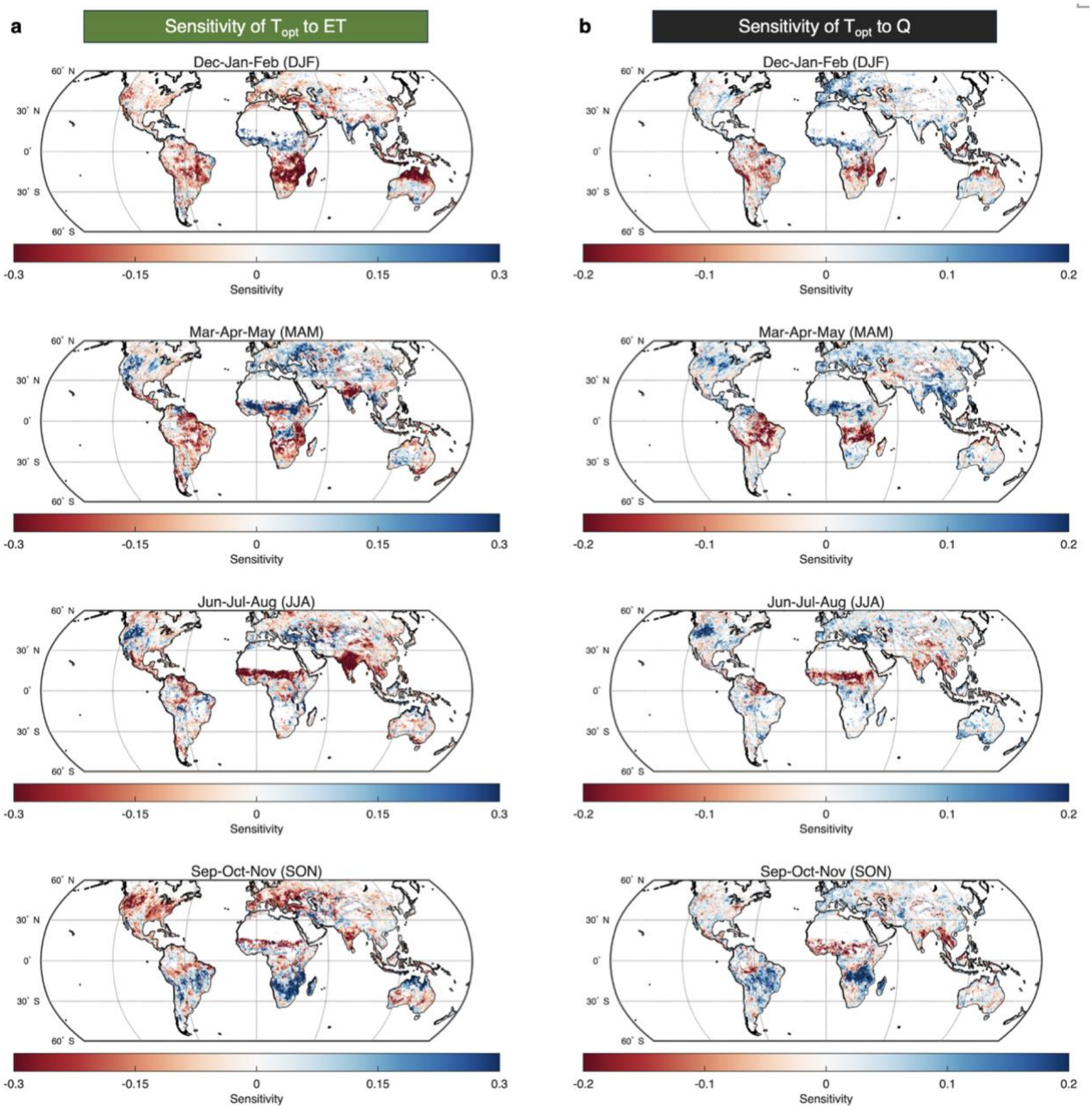

Supplementary Fig. 10.
Spatial distributions of seasonal sensitivities of groundwater response time (T_{opt}) to major land-atmospheric variables. a, Sensitivities of T_{opt} to evapotranspiration (ET) over Dec-Jan-Feb (DJF), Mar-Apr-May (MAM), Jun-Jul-Aug (JJA), and Sep-Oct-Nov (SON) (left panel). **b,** Sensitivities of T_{opt} to runoff (Q) over DJF, MAM, JJA, and SON (right panel).

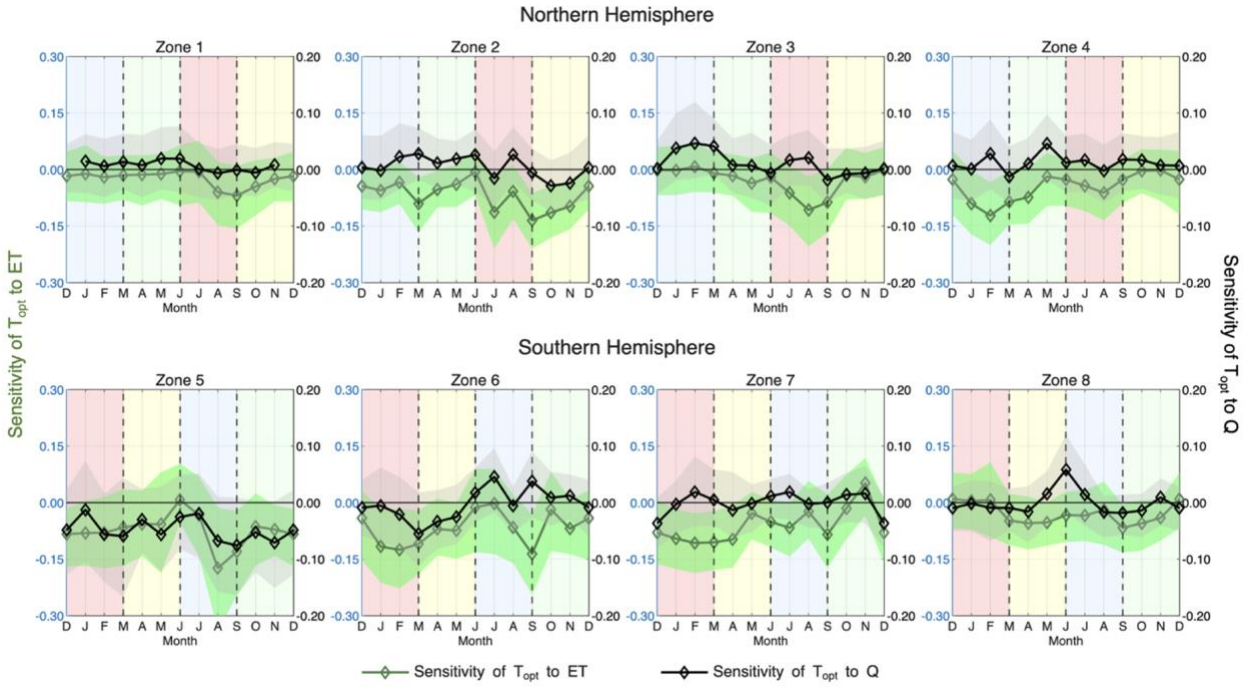

Supplementary Fig. 11.
Monthly variation of seasonal sensitivities of groundwater response time (T_{opt}) to major land-atmospheric variables for selected zones. Monthly sensitivities of T_{opt} to evapotranspiration (ET) (green marker lines and shaded areas) and runoff (Q) (black marker lines and shaded areas) for four selected zones in the Northern Hemisphere, including hotspots (Zone 1 and 3) and non-hotspots (Zone 2 and 4) (upper panel), and four selected zones in the Southern Hemisphere, including hotspots (Zone 6 and 7) and non-hotspots (Zone 5 and 8) (lower panel), as characterized in Supplementary Fig. 6. The marker lines represent the ensemble mean of all pixels within the selected zones, and the shaded areas represent the uncertainty ranges between the 25th and 75th percentiles.

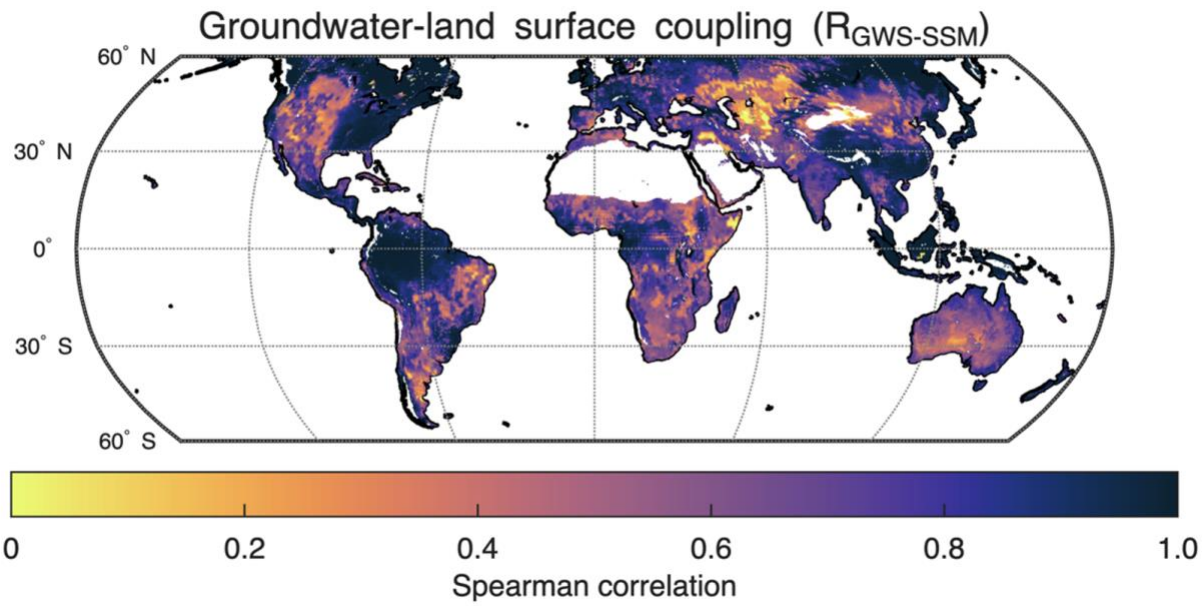

Supplementary Fig. 12.
Spatial distribution of groundwater-land surface coupling ($R_{GWS-SSM}$). The groundwater-land surface coupling is expressed by Spearman's correlation coefficient (R), with higher values indicating stronger coupling.

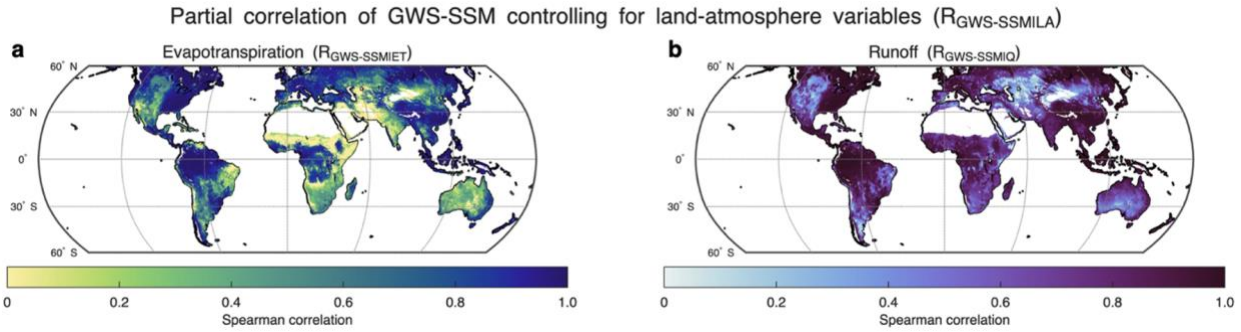

Supplementary Fig. 13.
Spatial distributions of partial correlation of groundwater-land surface controlling for major land-atmospheric variables ($R_{GWS\text{-}SSM|LA}$). a, b, Spatial distribution of partial correlation, expressed by Spearman's correlation coefficient (R), of GWS-SSM controlling for **a,** evapotranspiration ($R_{GWS\text{-}SSM|ET}$), and **b,** runoff ($R_{GWS\text{-}SSM|Q}$).

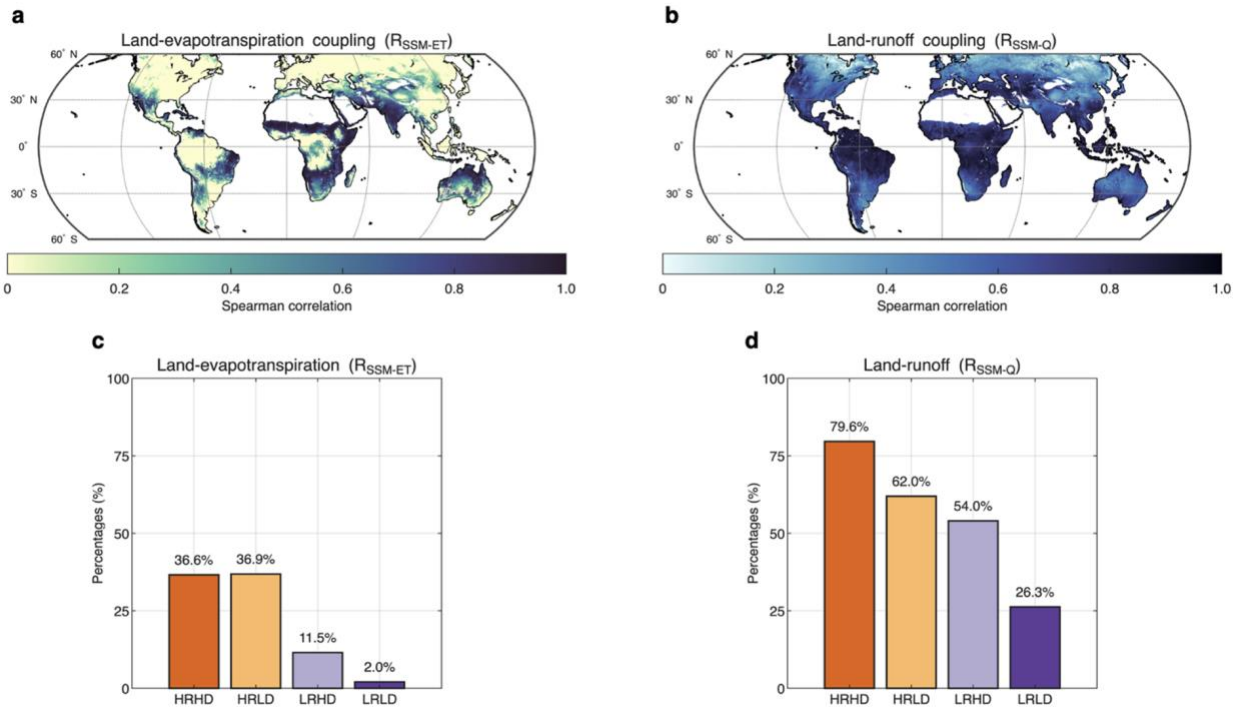

Supplementary Fig. 14.
Land-atmosphere coupling (R_{SSM-LA}) across association types. a, Land-evapotranspiration coupling, expressed by Spearman's correlation coefficient (R) of SSM-ET (R_{SSM-ET}), over Dec-Jan-Feb (DJF), Mar-Apr-May (MAM), Jun-Jul-Aug (JJA), and Sep-Oct-Nov (SON) (left panel). **b,** Land-runoff coupling, expressed by Spearman's correlation coefficient (R), of SSM-Q (R_{SSM-Q}), over DJF, MAM, JJA, and SON (right panel). **c, d,** Bar charts illustrate the contributions of these couplings between land surface and **c,** evapotranspiration (R_{SSM-ET}), and **d,** runoff (R_{SSM-Q}), for each association type (in percentages).

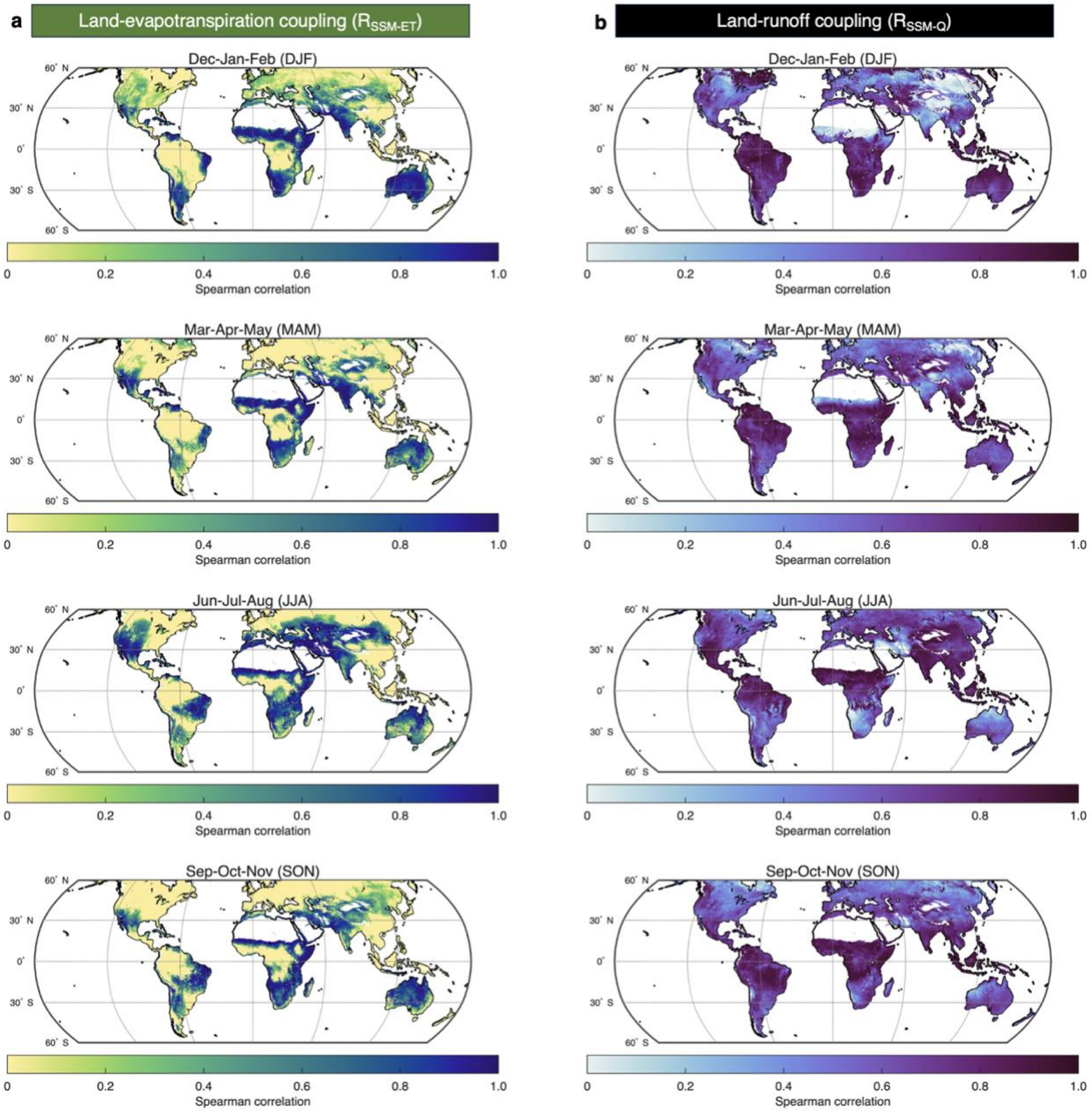

Supplementary Fig. 15.

Spatial distributions of seasonal land-atmosphere coupling (R_{SSM-LA}). a, Land-evapotranspiration coupling, expressed by Spearman's correlation coefficient (R) of SSM-ET (R_{SSM-ET}), over Dec-Jan-Feb (DJF), Mar-Apr-May (MAM), Jun-Jul-Aug (JJA), and Sep-Oct-Nov (SON) (left panel). **b,** Land-runoff coupling, expressed by Spearman's correlation coefficient between SSM-Q (R_{SSM-Q}), over DJF, MAM, JJA, and SON (right panel).

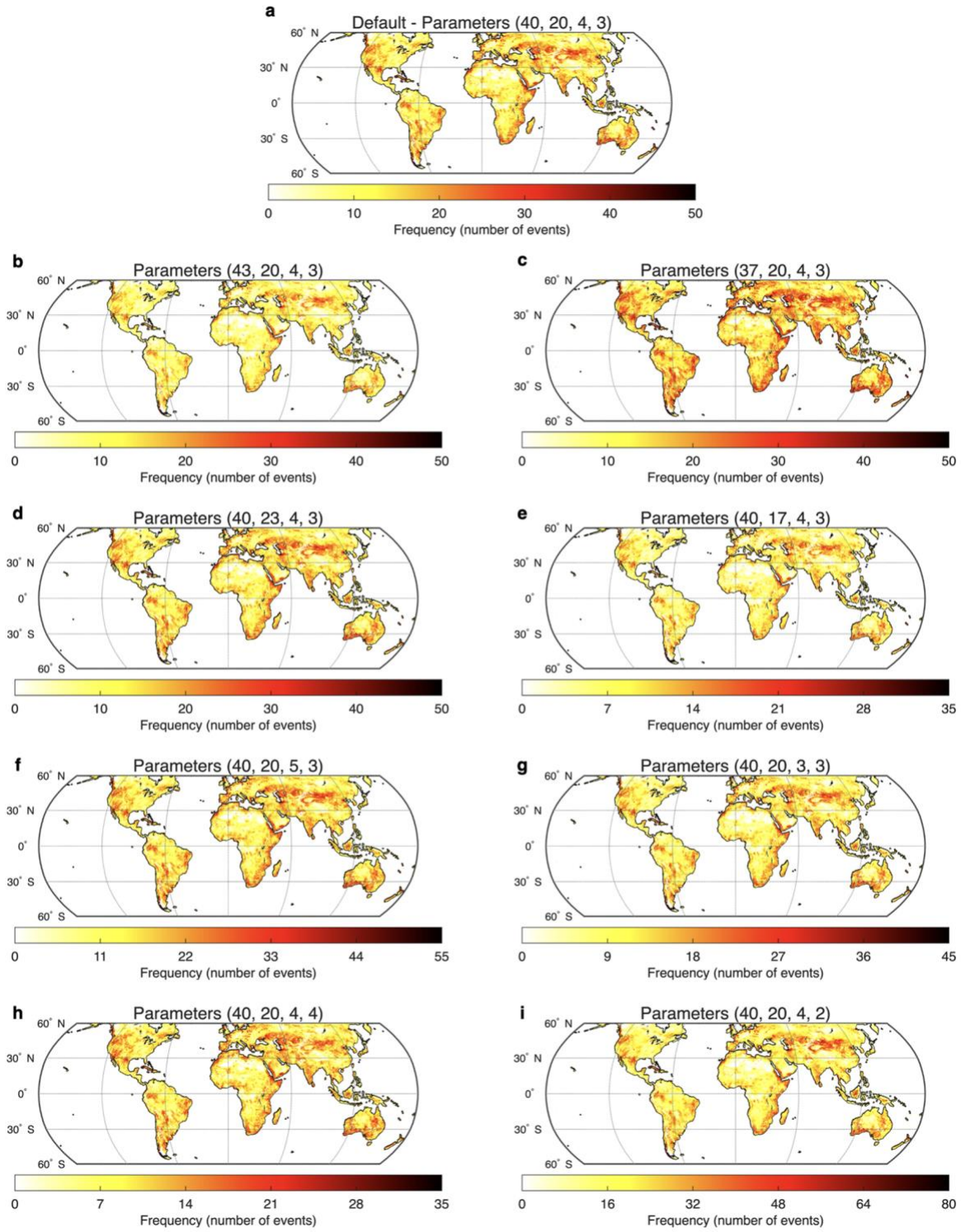

Supplementary Fig. 16.
Sensitivity analysis for the parameter thresholds in the flash drought definition. a, The default thresholds set for the used flash drought definition (onset point – 40th percentile, persistence point – 20th percentile, development period – 4 pentads, persistence period – 3 pentads, Supplementary Fig. 3). **b,c,** Adjusting thresholds of the first parameter (onset point). **d,e,** Adjusting thresholds of the second parameter (persistence point). **f,g,** Adjusting thresholds of the third parameter (development period). **h,i,** Adjusting thresholds of the fourth parameter (persistence period).